

Ab initio molecular dynamics study of H₂ adsorption on sulfur- and chlorine-covered Pd(100)

Axel Groß

Institut für Theoretische Chemie, Universität Ulm, 89069 Ulm/Germany

The adsorption of molecular hydrogen on sulfur- and chlorine-covered Pd(100) in a (2×2) geometry is studied by ab initio molecular dynamics simulations. The potential energy surfaces of H₂/S(2×2)/Pd(100) and H₂/Cl(2×2)/Pd(100) are rather similar. Consequently, also the dependence of the sticking probability on incident kinetic energy, angle of incidence and internal excitations are very close. For H₂/S(2×2)/Pd(100), previous results obtained on an interpolated ab initio potential energy surface are confirmed, except for the dependence of the sticking probability on the initial rotational state which exhibits a surprising rotational enhancement. Discrepancies with respect to the experiment remain which are discussed. In the simulations, several subsurface penetration events have been found, preferentially close to the sulfur or chlorine adatoms, respectively. This is explained by lower barriers caused by the destabilization of hydrogen adsorption close to the repulsive adatoms.

Keywords: palladium, hydrogen, density functional theory calculations, poisoning, adsorption dynamics, subsurface penetration

I. INTRODUCTION

Under realistic ambient conditions, almost every surface or substrate is covered with adsorbates. These adsorbates can have a significant influence on the chemical and catalytic activities of surfaces. They do not only lead to the blocking of adsorption sites, but can interact directly or indirectly [1] through the substrate with further adsorbates. Thus they can either promote [2] or poison [3] chemical reactions at surfaces. The most prominent catalyst poison is lead whose presence deactivates the car exhaust catalyst [4], but also sulfur is well-known to poison catalysts such as Pd-containing Diesel oxidising catalyst [5, 6] or palladium catalysts for methane combustion [7].

The first and often rate-limiting step in surface reactions is the adsorption of the reactants. Therefore studying the adsorption of molecules on surfaces precovered with adsorbates is of considerable relevance for a complete understanding of surface reactions and their poisoning or promotion. The influence of adsorbates on the adsorption properties for further adsorbates has been the topic of numerous theoretical electronic structure studies (see, e.g., [1, 8–16]). As far as the theoretical treatment of the adsorption dynamics on precovered surfaces is concerned, however, there have been up to now only relatively few studies [17–21]. This has been due to the fact that the presence of coadsorbates increases the complexity of surface structures which in particular increases the computational efforts for dynamical studies based on quantum methods [22, 23].

Hydrogen adsorption has often been used as a model system to study the principles of adsorption processes [24, 25]. For example, the interaction of H₂ with sulfur-covered Pd surfaces was used as a model system for the study of dissociative adsorption poisoned by a coadsorbate [19, 26–29]. According to electronic structure calculations based on density functional theory (DFT),

the adsorption of sulfur turns the non-activated dissociative adsorption of H₂ into an activated one [1, 8–10]. This is caused by a combination of direct repulsion for H₂ close to the adsorbed sulfur atoms and indirect interaction through the sulfur-induced modification of the electronic structure of Pd(100). Dynamical studies performed on a potential energy surface (PES) based on an interpolation of DFT data showed a typical activated behavior with the sticking probability increasing significantly at energies above the minimum barrier height [17, 18]. These findings were at variance with experimental molecular beam data which exhibited no pronounced activated behavior [26]. However, the dynamical simulations were able to reproduce the vibrational heating and rotational cooling observed in D₂ desorption from Pd(100) [19].

In this work, I present ab initio molecular dynamics (AIMD) simulations of H₂ impinging on S(2×2)/Pd(100) in which the forces necessary to integrate the classical equations of motion are calculated “on the fly” in each step by periodic DFT calculations. Some years ago, AIMD simulations of molecules interacting with surfaces have been restricted to a small number of trajectories [30, 31] due to their high numerical effort. Because of the increase in computer power and the development of efficient algorithms it has now become possible to run a statistically meaningful number of DFT-based AIMD trajectories for the determination of reaction probabilities [20, 32–35]. This allows to determine reaction probabilities on complex surface structures involving several reaction partners since no interpolation scheme is required. This also avoids artefacts that can be introduced through the interpolation method. Thus we can assess the quality of simulations performed on interpolated PESs. In addition, we can address further aspects in the interaction dynamics such as the influence of the surface motion on reaction probabilities. In addition, the AIMD simulations can be used as a means for an unbiased search for reaction mechanisms. This will be illustrated using

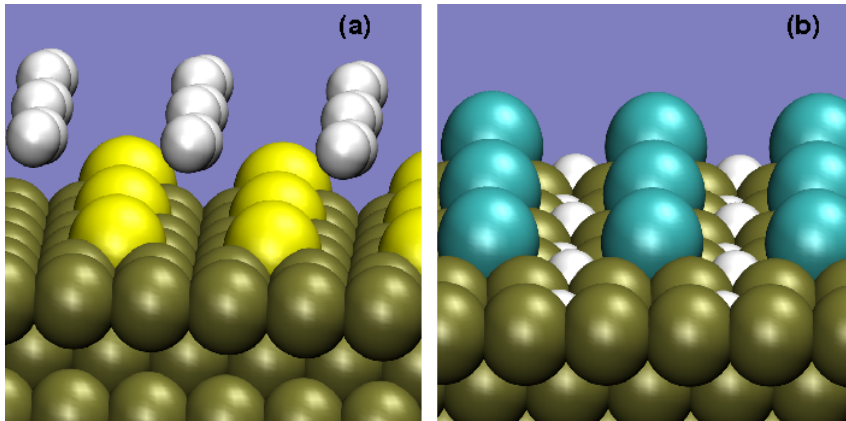


FIG. 1: Snapshots of ab initio molecular dynamics simulations of H_2 impinging on a) $\text{S}(2 \times 2)/\text{Pd}(100)$ (left panel) and b) $\text{Cl}(2 \times 2)/\text{Pd}(100)$ (right panel) within a 2×2 periodicity. Panel a illustrates the initial configuration with the H_2 molecule 5 \AA above the Pd layer whereas panel b depicts a situation after dissociative adsorption.

subsurface penetration events that have been observed in the simulations.

Furthermore, I have performed AIMD simulations of the H_2 adsorption on $\text{Cl}(2 \times 2)/\text{Pd}(100)$. Chlorine can also act as a poison, for example in the CO oxidation on supported Au particles [13, 36]. Chlorine is also present as a specifically adsorbed species at electrochemical electrode/electrolyte interfaces if perchloric acid solution is used as the electrolyte. It has been shown that the presence of adsorbed chlorine can strongly influence the adsorption properties of electrodes [37]. Hence this study is also of relevance for the understanding of the properties of electrode surfaces with specifically adsorbed anions.

II. THEORETICAL METHODS

All DFT calculations were performed using the Vienna ab initio simulation package (VASP) [38, 39] within the generalized gradient approximation (GGA) to describe the exchange-correlation effects, employing Perdew, Burke and Ernzerhof (PBE) exchange-correlation functional [40]. The ionic cores are represented by projector augmented wave (PAW) potentials [41] as constructed by Kresse and Joubert [42]. The electronic one-particle wave functions are expanded in a plane-wave basis set up to a cutoff energy of 280 eV.

The AIMD simulations were performed within the microcanonical ensemble using the Verlet algorithm with a time step of 1 fs within a 2×2 supercell. The substrates were modeled by a 5-layer Pd(100) slab with an adsorbate coverage of sulfur and chlorine, respectively, of $1/4$. All atoms were allowed to move except for the lowest two layers of the Pd(100) which were fixed at their bulk positions.

The trajectories were started with random initial lateral positions and orientations of the H_2 molecule 5 \AA above the surface with the substrate atoms initially at rest. Such a situation is illustrated for H_2 impinging

on $\text{S}(2 \times 2)/\text{Pd}(100)$ in Fig. 1a. Sticking probabilities for each considered structure and incident kinetic energy were evaluated by averaging over at least 150 trajectories. A trajectory was considered to correspond to a dissociation event when the interatomic distance of the molecule exceeded 2.5 \AA (depicted in Fig. 1b for H_2 on $\text{Cl}(2 \times 2)/\text{Pd}(100)$) and to a scattering event when the molecule returned to the initial distance of 5 \AA from the surface. Because of the stochastic nature of the sticking process [32], the statistical error of the sticking probabilities is given by $\sigma = \sqrt{S(1-S)}/\sqrt{N}$ where S is the sticking probability and N the number of trajectories [43]. For $N \geq 150$, the statistical error is $\sigma \leq 0.04$. It is important to emphasize that the statistical error does not depend on the complexity of the system, i.e., on the number of considered dynamical degrees of freedom, but only on the number of calculated trajectories.

In order to find the minimum energy paths and the barrier height for the subsurface penetration of hydrogen, we have used an automatic search routine, the climbing image nudged-elastic band (NEB) method [44, 45], as implemented in the VASP code.

III. RESULTS AND DISCUSSION

A. Potential energy surfaces

First, we address the potential energy surfaces (PES). The PES of H_2 interacting with $\text{S}(2 \times 2)/\text{Pd}(100)$ has been previously mapped out in great detail [1, 8–10]. The presence of a (2×2) sulfur adlayer turns the not-activated $\text{H}_2/\text{Pd}(100)$ system into an activated one. The interaction of the adsorbed sulfur atoms with hydrogen is characterized by a strong repulsion, as far as the direct sulfur-hydrogen interaction is concerned, and a longer-range indirect repulsive effects through the sulfur-induced change of the electronic properties of the Pd

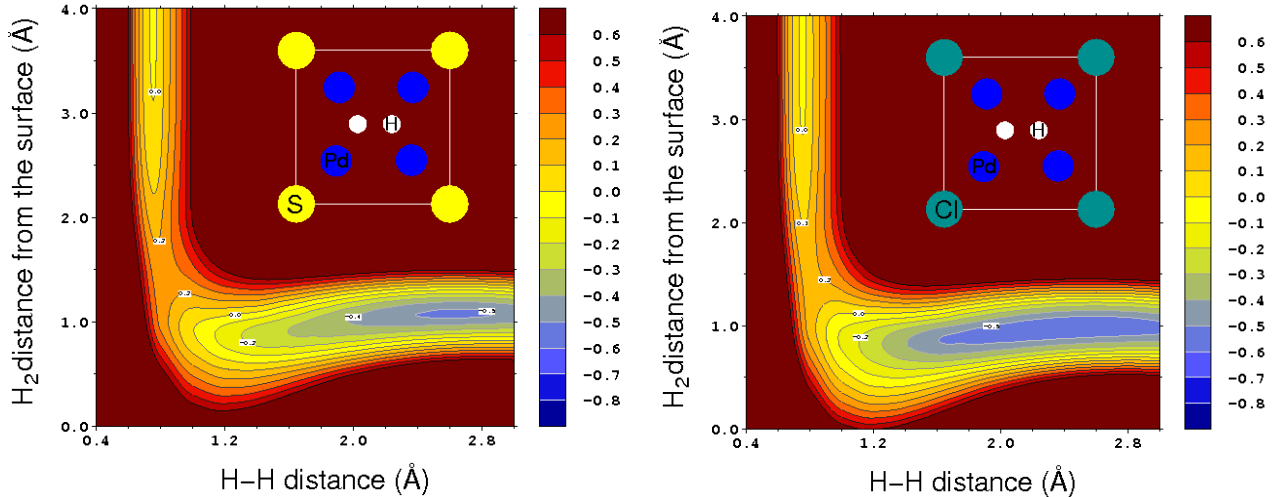


FIG. 2: Two-dimensional cut through the potential energy surface of H_2 interacting with $S(2 \times 2)/Pd(100)$ and $Cl(2 \times 2)/Pd(100)$ as a function of the H_2 of center distance from the surface and the H-H distance. The configuration of the remaining degrees of freedom is indicated in the insets. The level spacing is 0.1 eV.

atoms [1]. The minimum barrier is at a location at the fourfold-hollow site furthest away from the sulfur atoms. A corresponding two-dimensional cut through the PES is plotted in Fig. 2 together with an illustration of the atomic geometries. Note that the height of the minimum barrier of about 250 meV is 100 meV higher than in previous studies [1, 8–10]. This is caused by the different computational setup: in the previous studies the PES has been calculated for a symmetric three-layer slab with hydrogen adsorption on both sides using a full-potential-linear-augmented-plane-wave (FP-LAPW) method whereas here a five-layer slab with adsorption only on one side was used. Furthermore, in the previous studies also a slightly different GGA functional, the Perdew-Wang 91 [46] functional, was employed. However, apart from the height of the minimum barrier all features of the calculated PES are rather similar.

Figure 2 shows a two-dimensional cut through the $H_2/Cl(2 \times 2)/Pd(100)$ -PES for the same configuration as for the sulfur-covered surface. As sulfur, chlorine is an electron acceptor. And in fact, the PES of $H_2/Cl(2 \times 2)/Pd(100)$ bears a striking resemblance to the PES of $H_2/S(2 \times 2)/Pd(100)$, as Fig. 2 demonstrates. The most significant difference is that the minimum barrier height for dissociative adsorption is at about 180 meV, i.e., the poisoning effect of chlorine is a little bit less pronounced than for sulfur, but otherwise all features of the two PESs are almost the same, as an inspection of other two-dimensional cuts through the six-dimensional configuration confirms.

B. Ab initio molecular dynamics simulations

The sticking probability of H_2 impinging on $S(2 \times 2)/Pd(100)$ under normal incidence as a function of the kinetic energy is plotted in Fig. 3. The dash-dotted line shows the results of previous MD simulations on an interpolated PES. Apart from the shift of about 0.1 eV which is due to the different set-up of the electronic structure calculations (see previous section), the dependence of the sticking probability on the kinetic energy is rather similar. In the original interpolation, an artificial symmetry $\theta \leftrightarrow \pi - \theta$ was introduced since the total-energy calculation the interpolation was based on were only performed at high-symmetry points with respect to the lateral H_2 center-of-mass degrees of freedom [1]. Whereas the corresponding artificial symmetry has led to a significant quantitative error in the non-activated dissociation dynamics of H_2 on clean $Pd(100)$ [20, 21], for the activated system $H_2/S(2 \times 2)/Pd(100)$ these details apparently hardly matter, in particular because the minimum barrier is at a high-symmetry site. This indicates that for activated systems it is mainly the region around the minimum energy path that matters for the determination of the sticking probability. For non-activated systems, however, the dissociative adsorption can occur along many different paths which all need to be described accurately. This makes the interpolation of a non-activated PES much more challenging [47].

The similarity of the AIMD and the MD results also means that the discrepancy between the experimental molecular beam results [26] still remains. I have checked whether the surface recoil might play a role in the adsorption dynamics by performing AIMD simulations for an initial kinetic energy of $E_i = 400$ meV with the

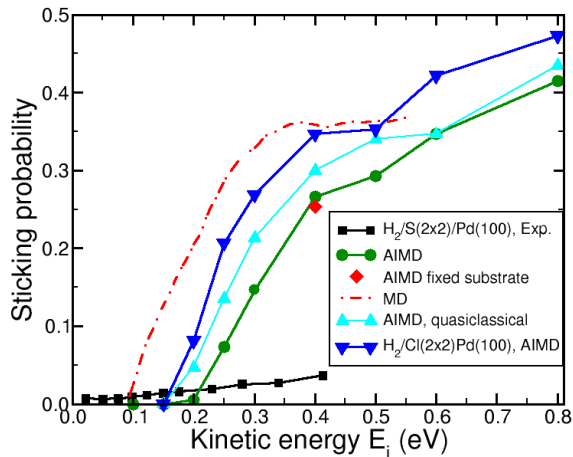


FIG. 3: Sticking probability of H_2 impinging on S-covered Pd(100) under normal incidence determined in classical and quasiclassical AIMD simulation. For $E_{\text{kin}} = 0.4 \text{ eV}$, additional AIMD runs with the substrate kept fixed were performed. In addition, the results of classical MD simulation [18] based on a parameterization of DFT results [1, 10] and measured sticking probabilities [26] are included. In addition, AIMD results for H_2 impinging on Cl-covered Pd(100) are included.

surface atoms kept fixed. The corresponding sticking probability (red diamond in Fig. 3) is only slightly reduced with respect to the simulations including surface recoil. Apparently the recoil of the surface atoms of the $\text{S}(2 \times 2)/\text{Pd}(100)$ substrate hardly matters as far as the adsorption dynamics is concerned. Note that this is different in the H_2 adsorption on hydrogen-precovered Pd(100) where the motion of the surface atoms has a significant influence on the sticking probability [21].

Quantum effects can also not explain the substantial difference between experimental and theoretical results for the sticking probability. Hence one can only speculate about the reasons for the discrepancy. As previously discussed [18], they might be due to the fact that in the experiment no well-ordered (2×2) sulfur-adlayer was present.

Figure 3 also shows the results of quasiclassical AIMD simulations, i.e. classical simulations in which the H_2 molecules initially vibrate with a vibrational energy corresponding to the H_2 zero-point energy [48, 49]. The quasiclassical AIMD results are slightly larger than the purely classical AIMD results. This indicates that there is a vibrational enhancement in the sticking probability which is consistent with the observed vibrational heating in desorption [19]. However, at first glance this seems to be surprising since the potential energy surface plotted in Fig. 2 indicates that the $\text{H}_2/\text{S}(2 \times 2)/\text{Pd}(100)$ is an early-barrier system, i.e. the barrier is located before the curved region of the minimum energy path towards dissociation, and according to the Polanyi rules [50] in such a system no vibrational effects in the reaction probability should be expected. However, at the position of

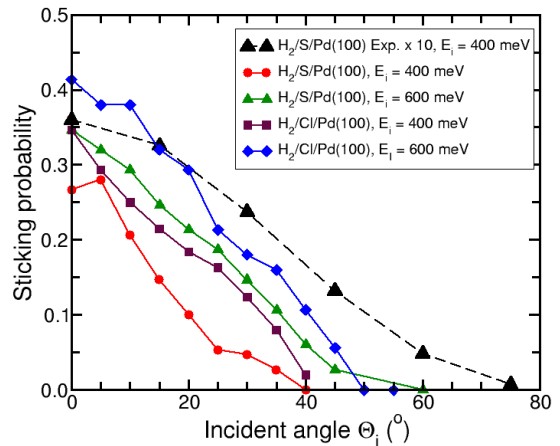


FIG. 4: Calculated sticking probabilities for H_2 impinging on S- and Cl-covered Pd(100) as a function of the angle of incidence for two initial kinetic energies, $E_{\text{kin}} = 0.4 \text{ eV}$ and $E_{\text{kin}} = 0.6 \text{ eV}$. In addition, experimental results for $\text{H}_2/\text{S}/\text{Pd}(100)$ are included [26] which have been scaled by a factor of 10 in order to make the comparison easier.

the dissociation barrier the H-H stretch frequency is already lowered, and such a lowering of the H-H vibrational frequency leads to vibrational adiabatic effects which enhance the sticking probability [51].

The sticking probability of H_2 impinging on $\text{Cl}(2 \times 2)/\text{Pd}(100)$ based on classical AIMD simulations is also included in Fig. 3. The AIMD sticking curves for $\text{H}_2/\text{S}(2 \times 2)/\text{Pd}(100)$ and $\text{H}_2/\text{Cl}(2 \times 2)/\text{Pd}(100)$ are rather similar, both curves even have a kink at $E_i \approx 500 \text{ meV}$. The main difference is that at lower kinetic energies the $\text{H}_2/\text{Cl}(2 \times 2)/\text{Pd}(100)$ sticking curve is shifted by 50 – 100 meV to lower energies compared to the sticking curve for $\text{H}_2/\text{S}(2 \times 2)/\text{Pd}(100)$. This just reflects the fact that the potential energy surfaces exhibit very similar features, only the energy minimum barrier for dissociative adsorption is smaller by 70 meV for $\text{H}_2/\text{Cl}(2 \times 2)/\text{Pd}(100)$.

Due to the presence of the repulsive adatoms, the potential energy surfaces of $\text{H}_2/\text{S}(2 \times 2)/\text{Pd}(100)$ and $\text{H}_2/\text{Cl}(2 \times 2)/\text{Pd}(100)$ exhibit a strong variation as a function of the lateral coordinates of the H_2 molecules, i.e., the potential energy surfaces are strongly corrugated. This corrugation is reflected in the strong dependence of the sticking probability on the angle of incidence [52–54] which is plotted in Fig. 4 for the two considered systems for two incident kinetic energies, $E_i = 400$ and 600 meV . For $\text{H}_2/\text{S}(2 \times 2)/\text{Pd}(100)$, in addition the results of the molecular beam experiment [26] for $E_i = 400 \text{ meV}$ are plotted which are scaled by a factor of ten in order to make a comparison with the trends in the theoretical results easier. Again, the AIMD results for $\text{H}_2/\text{S}(2 \times 2)/\text{Pd}(100)$ are rather similar with respect to the results of previous MD simulations [18]. And also the AIMD results for $\text{H}_2/\text{S}(2 \times 2)/\text{Pd}(100)$ and

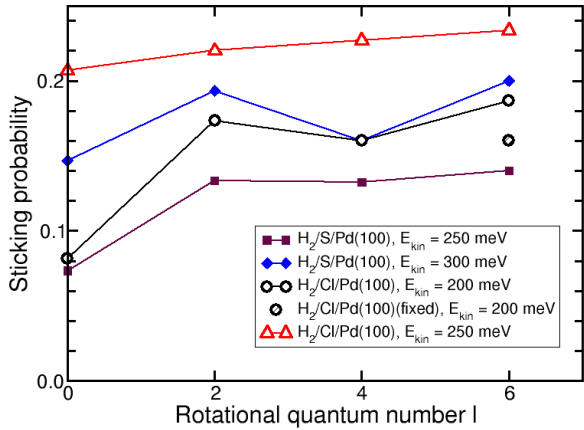


FIG. 5: Sticking probability of H_2 impinging on S- and Cl-covered Pd(100) under normal incidence determined as a function of the initial rotational state for two initial kinetic energies closely above the minimum barrier height. For $H_2/Cl(2 \times 2)/Pd(100)$, additional AIMD runs with the substrate atoms kept fixed were performed.

$H_2/Cl(2 \times 2)/Pd(100)$ are comparable except for the fact that on $Cl(2 \times 2)/Pd(100)$ the sticking probabilities are a little bit larger because of the smaller energy minimum barrier. Because of the large corrugation, additional parallel momentum leads to a suppression of the sticking probability [18]. Qualitatively, the suppression for higher angles of incidence is stronger in the theory than in the experiment. This might be another hint that in the experiment the sulfur-covered surface is not well-ordered so that there is a significant fraction of less-corrugated parts on the surface.

Typically, in the desorption of diatomic molecules from surfaces, rotational cooling is observed, i.e. the mean rotational energy of desorbing molecules is less than expected in thermal equilibrium [19, 55, 56]. Invoking the principle of time reversal or detailed balance, the rotational cooling in desorption is associated with rotational hindering in adsorption which can be more intuitively understood: Rotating molecules might rotate out of favorable configurations for dissociative adsorption leading to a reduced dissociative adsorption probability. In fact, this rotational hindering has been directly observed in molecular beam experiments of H_2 molecules impinging on Pd(111) [57, 58]. Only in the system $H_2/Pd(110)$, a rotational enhancement of the sticking probability has been predicted based on ab initio-based quantum dynamics simulations [59]. This rotational enhancement has been attributed to the strong corrugation and anisotropy of the potential energy surface.

In Fig. 5, I plot the calculated sticking probability based on AIMD simulations of H_2 impinging on $S(2 \times 2)/Pd(100)$ and $Cl(2 \times 2)/Pd(100)$ as a function of the initial rotational state. The initial rotational energy has been selected according to the particular quantum

state; the initial orientations of the molecular axis and of the rotational momentum have been chosen randomly. The initial kinetic energies are larger than but close to the minimum barrier height so that the time-reverse dynamics corresponds to typical desorption events.

Surprisingly enough, the calculated sticking probabilities do not exhibit any rotational hindering. In contrast, the smallest sticking probabilities are obtained for initially non-rotating molecules. Consequently, additional rotational motion obviously enhances the sticking probability. Again, the sticking probabilities at sulfur- and chlorine-covered Pd(100) are very similar except for the difference in the minimum barrier height. Note that the AIMD results are at variance with the previous MD results for $H_2/S(2 \times 2)/Pd(100)$ on an interpolated potential energy surface [18].

Recall that in these MD simulations all substrate atoms were kept fixed. In order to check whether this has a significant influence on the sticking probability for initially rotating molecules, I performed additional AIMD simulations for H_2 on $Cl(2 \times 2)/Pd(100)$ initially rotating according to the $l = 6$ rotational state with all substrate atoms kept fixed. The resulting sticking probability also included in Fig. 5 is only slightly reduced with respect to the unconstrained AIMD simulations. In any case, the reduction is not sufficient to explain the qualitatively different dependence of the sticking probability on the initial rotational state.

Obviously, the artificial symmetry $\theta \leftrightarrow \pi - \theta$ contained in the interpolated PES which did not matter for the determination of the sticking probability of initially non-rotating molecules affects the sticking probability if the molecules initially rotate and hence explore a larger region of the configuration space. And here, as in the system $H_2/Pd(110)$ [59], the strong corrugation and anisotropy of the potential energy surface leads to an efficient coupling of the rotational motion to the motion along the reaction path towards dissociative adsorption. Note that rotational enhancement in dissociative adsorption can also result from rotational adiabatic effects due to the elongation of the molecular bond and the accompanying increase in the moment of inertia [60, 61] but this mechanism should not be operative in the early-barrier systems considered here.

The rotational enhancement in the dissociative adsorption is also in a seeming conflict with the experimentally observed rotational cooling in hydrogen desorption from $S(2 \times 2)/Pd(100)$ [19] invoking the principle of detailed balance. However, it is important to note that the principle of detailed balance couples adsorption and desorption at a particular coverage and temperature [30, 62], and typically adsorption experiments are performed on clean surfaces at low temperatures whereas desorption fluxes are measured at high surface temperatures and coverages.

It should also be mentioned that in the $D_2/S/Pd(100)$ desorption experiments yielding rotational cooling the deuterium atoms are supplied to the surface by atomic

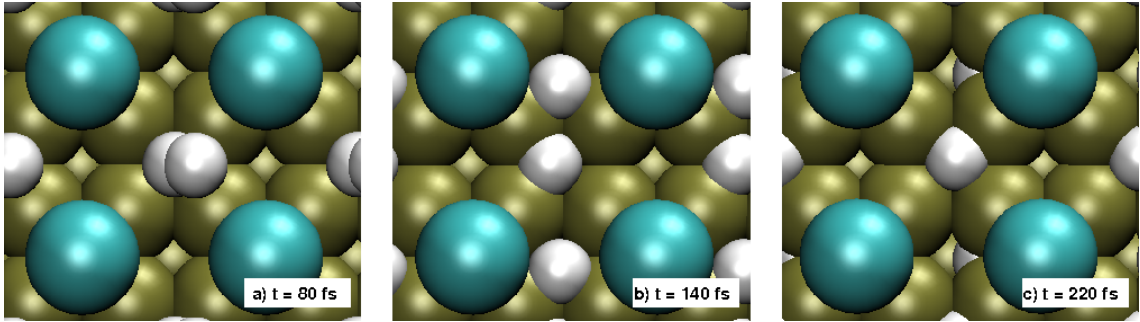


FIG. 6: Snapshots of the subsurface penetration of hydrogen on $\text{Cl}(2 \times 2)/\text{Pd}(100)$ taken from an ab initio molecular dynamics simulation at $t = 80$ fs (a), $t = 140$ fs (a) and $t = 220$ fs (a). The H_2 molecule was impinging on the chlorine-covered $\text{Pd}(100)$ surface with an initial kinetic energy of $E_i = 200$ meV and an initial rotational energy corresponding to the $l = 6$ rotational state.

permeation through the bulk [19, 28, 29]. This means that before desorption, the deuterium atoms originate from subsurface layers. However, it is unclear whether before desorption the atoms equilibrate on the surface or whether they directly find a partner for the associative desorption after they appear on the surface.

Hence it is also interesting to address the time-reverse process of the permeation towards the surface, namely the subsurface penetration of hydrogen at sulfur- and chlorine-covered $\text{Pd}(100)$. This process is also interesting in the context of hydrogen storage. Although palladium is not considered as a material for hydrogen storage because of its large specific mass, it still is used as a model system to study hydrogen absorption in metals [63]. In addition, thin palladium films act as hydrogen-insertion promoters for complex hydrides formed by light elements [64, 65]. Furthermore, subsurface penetration of hydrogen in Pd nanoparticles might be the crucial promoter for the olefin hydrogenation [66].

Clean $\text{Pd}(100)$ exhibits a relatively small barrier of 0.41 eV hindering the subsurface penetration of a single hydrogen atom [25]. Recently however, it has been shown that the subsurface penetration on hydrogen-covered $\text{Pd}(100)$ is substantially facilitated if the subsurface penetration occurs in a concerted fashion with the adsorption site that is emptied immediately being refilled by another hydrogen atom from an adjacent bridge site [67].

Yet, in the AIMD simulations of H_2 impinging on sulfur- and chlorine-covered $\text{Pd}(100)$ subsurface penetration events occurred that did not involve any concerted mechanism. In Fig. 6, such a typical subsurface penetration event is illustrated using snapshots of an AIMD trajectory. The H_2 molecule is impinging on $\text{Cl}(2 \times 2)/\text{Pd}(100)$ with an initial kinetic energy of $E_i = 200$ meV and an initial rotational energy corresponding to the $l = 6$ rotational state (Fig. 6a). The H_2 molecule directly dissociates and the two hydrogen atoms populate two adjacent four-fold hollow adsorption sites (Fig. 6b). The hydrogen atom at the four-fold hollow site between the two chlorine atoms then almost directly

enters the tetragonal subsurface site (Fig. 6c). In fact, at lower kinetic energies subsurface penetration events have exclusively occurred at the four-fold hollow site between the sulfur or chlorine atoms, respectively, only at higher kinetic energy ≥ 600 meV the penetration into the bulk also occurred at the central four-fold hollow site.

In order to rationalize this facile subsurface penetration, as a first step I calculated the energetics of hydrogen at the available adsorption and subsurface sites of the sulfur- and chlorine covered surface. As a reference, I determined the same numbers for the clean $\text{Pd}(100)$ surface which indeed compare favorably with previous results [25]. These energies are collected in Tab. I. With respect to the four-fold adsorption and the tetraeder subsurface site, there are two inequivalent position within the (2×2) surface unit cell, one at or close to the center of the surface unit cell furthest away from the sulfur or chlorine atom, respectively, denoted by center in Tab. I, and one close to the adsorbed heteroatoms denoted by bridge in Tab. I. The octaeder subsurface site is directly below the Pd atoms which are all equivalent within this surface unit cell.

With respect to the hydrogen adsorption sites on the surface, the repulsive nature of the sulfur and chlorine atoms is reflected in the fact that the binding of the H atoms is weaker at the sites close to the adatoms. Sulfur is more repulsive than chlorine since the binding energy is lowered by 0.22 eV close to the S atoms whereas it is only lowered by 0.16 eV close to the Cl atoms. The repulsive influence of the electronegative adatoms reaches down to the subsurface tetraeder site where the sites close to adatoms are less favorable by 0.09 eV and 0.05 eV for $\text{S}(2 \times 2)/\text{Pd}(100)$ and $\text{Cl}(2 \times 2)/\text{Pd}(100)$, respectively, compared to the more central tetraeder site. The subsurface octaeder site is at the height of the second Pd layer. Its occupation on the pre-covered surfaces is energetically slightly more favorable than on clean $\text{Pd}(100)$. This can be attributed to the fact that the destabilization of the surface sites on the (2×2) -covered surfaces is larger than the destabilization of the octaeder sites.

The subsurface penetration is in general not only en-

TABLE I: Adsorption and subsurface absorption energies E_b of hydrogen atoms on $S(2 \times 2)/Pd(100)$, $Cl(2 \times 2)/Pd(100)$ and $Pd(100)$ for a hydrogen coverage of $\Theta_H = 0.25$. For every surface, the most favorable adsorption site serves as the energy reference. The activation energies E_a correspond to the energy barriers for accessing the next subsurface site. For the assignment of the sites, see the text.

site	$S(2 \times 2)/Pd(100)$		$Cl(2 \times 2)/Pd(100)$		Pd(100)	
	E_b (eV)	E_a (eV)	E_b (eV)	E_a (meV)	E_b (eV)	E_a (eV)
Surface H: 4-fold center	0.0	0.45	0.0	0.34	0.0	0.41
Surface H: 4-fold bridge	0.22	0.28	0.16	0.25		
Subsurface H: tetraeder center	0.35	0.08	0.29	0.11	0.36	0.06
Subsurface H: tetraeder bridge	0.44	0.01	0.34	0.05		
Subsurface H: octaeder	0.28		0.30		0.32	

ergetically unfavorable, but also further kinetically hindered due to the presence of barriers. In Tab. I, I have also included the activation barriers for accessing the next subsurface sites. Whereas on the clean surface the barrier to propagate towards the tetraeder subsurface site is 0.41 eV, it is only 0.28 eV and 0.25 eV from the four-fold hollow sites close to the adsorbed sulfur and chlorine atom, respectively. The reduction in the barrier heights is closely related to the destabilization of the initial state that corresponds to H adsorption in the four-fold hollow sites close to the adatoms. On the central four-fold hollow site, the barrier height is slightly increased upon sulfur adsorption and slightly lowered upon chlorine adsorption, compared to clean Pd(100).

With respect to the observed facile subsurface penetration on the $S(2 \times 2)/Pd(100)$ and $Cl(2 \times 2)/Pd(100)$ surfaces, based on the energies listed in Tab. I the following scenario evolves: Upon H_2 dissociative adsorption on the (2×2) -covered Pd(100) surface, the two hydrogen atoms have to enter two adjacent four-fold hollow adsorption sites which are inequivalent. The one being closer to the adsorbed adatom is less favorable by about 0.2 eV. This destabilization of the adsorption site leads to a lowering of the subsurface penetration barriers by about 0.15 eV and thus to a facile subsurface penetration, since the first subsurface site, the tetraeder site, is less affected by the presence of the adatoms.

Still, it should be noted that the barrier for the concerted subsurface penetration on hydrogen-covered Pd(100) is only of the order of 0.1 eV [67], that means that it is even more facile than on sulfur- or chlorine-covered Pd(100). Finally one should also note that the number of observed subsurface penetration events in the AIMD simulations was too small in order to draw any conclusions about the time-reverse process, hydrogen permeation towards the surface.

IV. CONCLUSIONS

The interaction of molecular hydrogen with (2×2) sulfur- and chlorine covered Pd(100) has been studied using ab initio molecular dynamics simulations based on periodic density functional theory calculations. The

presence of sulfur and chlorine poisons hydrogen adsorption in a rather similar way, the potential energy surfaces of both systems look rather alike, except for the fact that the minimum barrier for H_2 adsorption on $Cl(2 \times 2)/Pd(100)$ is about 70 meV lower than on $Cl(2 \times 2)/Pd(100)$. As a consequence, the dependence of the sticking probability on incident kinetic energy, angle of incidence and internal excitations for both surfaces is very similar for both substrates.

For H_2 impinging on $S(2 \times 2)/Pd(100)$, the sticking probabilities for initially non-rotating molecules basically agree with previous molecular dynamics results on an interpolated potential energy surface, indicating that in this case the potential energy surface close to the minimum barrier configuration matters. For initially rotating molecules, however, the AIMD simulations show a qualitatively different dependence of the sticking probability on the initial rotational state than the previous MD simulations. This has been related to artefacts in the construction of the interpolated potential energy surface. According to the AIMD results, additional rotational motion increases the sticking probability which is at variance with the experimentally observed rotational cooling in desorption, invoking the principle of detailed balance. Possibly the adsorption conditions do not correspond to the experimental desorption conditions making the direct application of the principle of detailed balance not possible.

In the AIMD simulations, several subsurface penetration events of hydrogen atoms have been observed. The facile subsurface penetration has been rationalized on the basis of calculated minimum energy paths. The presence of the repulsive adatoms sulfur and chlorine leads to a larger destabilization of hydrogen adsorption sites on the surface than of the subsurface sites. This is accompanied by a lowering of the barriers towards subsurface penetration.

This work confirms that AIMD simulations have become a reliable and unbiased tool to study the dynamics of molecule-surface interactions yielding sometimes unexpected reaction and diffusion scenarios.

Acknowledgments

This work has been supported by the German Science Foundation (DFG) through the Research Unit 1376, contract GR 1503/21-1. Some of the calculations presented here were made possible through a grant of computer

time at the John von Neumann Institute for Computing in Jülich (contract hmu06). Additional computational resources have been provided by the stimulus programme “Electrochemistry for Electromobility” of the German Ministry of Education and Science (BMBF).

-
- [1] C. M. Wei, A. Groß, and M. Scheffler, *Phys. Rev. B* **57** (1998) 15572.
- [2] T. W. Hansen, J. B. Wagner, P. L. Hansen, S. Dahl, H. Topsøe, and C. J. H. Jacobsen, *Science* **294** (2001) 1508.
- [3] C. H. Bartholomew, *Applied Catalysis A: General* **212** (2001) 17 .
- [4] G. Acres and B. Harrison, *Top. Catal.* **28** (2004) 3.
- [5] X. Tiancun, A. Lidun, Z. Weimin, S. Shishan, and X. Guoxin, *Catal. Lett.* **12** (1992) 287.
- [6] T. Kolli, M. Huuhtanen, A. Hallikainen, K. Kallinen, and R. Keiski, *Catal. Lett.* **127** (2009) 49.
- [7] L. S. Escandón, S. Ordonez, A. Vega, and F. V. Diez, *Journal of Hazardous Materials* **153** (2008) 742 .
- [8] S. Wilke and M. Scheffler, *Surf. Sci.* **329** (1995) L605.
- [9] S. Wilke and M. Scheffler, *Phys. Rev. B* **53** (1996) 4926.
- [10] S. Wilke and M. Scheffler, *Phys. Rev. Lett.* **76** (1996) 3380.
- [11] J. J. Mortensen, B. Hammer, and J. Nørskov, *Phys. Rev. Lett.* **80** (1998) 4333.
- [12] B. Hammer, *Phys. Rev. B* **63** (2001) 205423.
- [13] P. Broqvist, L. M. Molina, H. Grönbeck, and B. Hammer, *J. Catal.* **227** (2004) 217.
- [14] S. Sakong and A. Groß, *J. Phys. Chem. A* **111** (2007) 8814.
- [15] L.-Q. Xue, X.-Y. Pang, and G.-C. Wang, *J. Phys. Chem. C* **111** (2007) 2223 .
- [16] D. R. Alfonso, *Topics Catal.* **55** (2012) 267.
- [17] A. Groß, C. M. Wei, and M. Scheffler, *Surf. Sci.* **416** (1998) L1095.
- [18] A. Groß and M. Scheffler, *Phys. Rev. B* **61** (2000) 8425.
- [19] M. Rutkowski, D. Wetzig, H. Zacharias, and A. Groß, *Phys. Rev. B* **66** (2002) 115405.
- [20] A. Groß and A. Dianat, *Phys. Rev. Lett.* **98** (2007) 206107.
- [21] A. Groß, *J. Chem. Phys.* **135** (2011) 174707.
- [22] A. Groß, *Surf. Sci.* **363** (1996) 1.
- [23] G.-J. Kroes, A. Groß, E. J. Baerends, M. Scheffler, and D. A. McCormack, *Acc. Chem. Res.* **35** (2002) 193.
- [24] A. Groß, *Surf. Sci.* **606** (2012) 690 .
- [25] P. Ferrin, S. Kandoi, A. U. Nilekar, and M. Mavrikakis, *Surf. Sci.* **606** (2012) 679 .
- [26] K. D. Rendulic, G. Anger, and A. Winkler, *Surf. Sci.* **208** (1989) 404.
- [27] M. L. Burke and R. J. Madix, *Surf. Sci.* **237** (1990) 1.
- [28] M. Rutkowski and H. Zacharias, *Phys. Chem. Chem. Phys.* **3** (2001) 3645.
- [29] M. Rutkowski, D. Wetzig, and H. Zacharias, *Phys. Rev. Lett.* **87** (2001) 246101.
- [30] A. Groß, M. Bockstedte, and M. Scheffler, *Phys. Rev. Lett.* **79** (1997) 701.
- [31] L. C. Ciacchi and M. C. Payne, *Phys. Rev. Lett.* **92** (2004) 176104.
- [32] A. Groß, *Phys. Rev. Lett.* **103** (2009) 246101.
- [33] A. Groß, *ChemPhysChem* **11** (2010) 1374.
- [34] A. Lozano, A. Groß, and H. F. Busnengo, *Phys. Chem. Chem. Phys.* **11** (2009) 5814.
- [35] A. Lozano, A. Groß, and H. F. Busnengo, *Phys. Rev. B* **81** (2010) 121402(R).
- [36] H.-S. Oh, J. Yang, C. Costello, Y. Wang, S. Bare, H. Kung, and M. Kung, *J. Catal.* **210** (2002) 375 .
- [37] M. Arenz, V. Stamenkovic, T. Schmidt, K. Wandelt, P. Ross, and N. Markovic, *Surf. Sci.* **523** (2003) 199 .
- [38] G. Kresse and J. Furthmüller, *Phys. Rev. B* **54** (1996) 11169.
- [39] G. Kresse and J. Furthmüller, *Comput. Mater. Sci.* **6** (1996) 15.
- [40] J. P. Perdew, K. Burke, and M. Ernzerhof, *Phys. Rev. Lett.* **77** (1996) 3865.
- [41] P. E. Blöchl, *Phys. Rev. B* **50** (1994) 17953.
- [42] G. Kresse and D. Joubert, *Phys. Rev. B* **59** (1999) 1758.
- [43] P. M. Agrawal, A. N. A. Samadh, L. M. Raff, M. T. Hagan, S. T. Bukkapatnam, and R. Komanduri, *J. Chem. Phys.* **123** (2005) 224711.
- [44] G. Henkelman and H. Jónsson, *J. Chem. Phys.* **113** (2000) 9978.
- [45] G. Henkelman, B. P. Uberuaga, and H. Jónsson, *J. Chem. Phys.* **113** (2000) 9901.
- [46] J. P. Perdew, J. A. Chevary, S. H. Vosko, K. A. Jackson, M. R. Pederson, D. J. Singh, and C. Fiolhais, *Phys. Rev. B* **46** (1992) 6671.
- [47] S. Lorenz, M. Scheffler, and A. Groß, *Phys. Rev. B* **73** (2006) 115431.
- [48] A. Groß and M. Scheffler, *J. Vac. Sci. Technol. A* **15** (1997) 1624.
- [49] H. F. Busnengo, C. Crespos, W. Dong, J. C. Rayez, and A. Salin, *J. Chem. Phys.* **116** (2002) 9005.
- [50] J. C. Polanyi and W. H. Wong, *J. Chem. Phys.* **51** (1969) 1439.
- [51] A. Groß and M. Scheffler, *Chem. Phys. Lett.* **256** (1996) 417.
- [52] G. R. Darling and S. Holloway, *Surf. Sci.* **304** (1994) L461.
- [53] A. Groß, *J. Chem. Phys.* **102** (1995) 5045.
- [54] A. Groß and M. Scheffler, *Chem. Phys. Lett.* **263** (1996) 567.
- [55] S. F. Shane, K. W. Kolasinski, and R. N. Zare, *J. Chem. Phys.* **97** (1992) 1520.
- [56] D. Wetzig, M. Rutkowski, H. Zacharias, and A. Groß, *Phys. Rev. B* **63** (2001) 205412.
- [57] M. Beutl, M. Riedler, and K. D. Rendulic, *Chem. Phys. Lett.* **247** (1995) 249.
- [58] M. Gostein and G. O. Sitz, *J. Chem. Phys.* **106** (1997) 7378.
- [59] A. Dianat and A. Groß, *J. Chem. Phys.* **120** (2004) 5339.

- [60] G. R. Darling and S. Holloway, *J. Chem. Phys.* **101** (1994) 3268.
- [61] A. Dianat and A. Groß, *Phys. Chem. Chem. Phys.* **4** (2002) 4126.
- [62] W. Brenig, A. Groß, and R. Russ, *Z. Phys. B* **96** (1994) 231.
- [63] A. Pundt and R. Kirchheim, *Annu. Rev. Mater. Res.* **36** (2006) 555.
- [64] J. Isidorsson, I. A. M. E. Giebels, H. Arwin, and R. Griessen, *Phys. Rev. B* **68** (2003) 115112.
- [65] C. Lebouin, Y. Soldo-Olivier, E. Sibert, M. De Santis, F. Maillard, and R. Faure, *Langmuir* **25** (2009) 4251.
- [66] M. Wilde, K. Fukutani, B. Ludwig, Wiebke Brandt, J.-H. Fischer, S. Schaueremann, and H.-J. Freund, *Angew. Chem. Int. Ed.* **47** (2008) 9289.
- [67] S. Sakong, C. Mosch, A. Lozano, H. F. Busnengo, and A. Groß, *ChemPhysChem* (2012) doi: 10.1002/cphc.201200526.